Journal of Catalysis **205,** 191–198 (2002)
doi:10.1006/jcat.2001.3434, available online at http://www.idealibrary.com on IDEAL®

Phosphorus-Doped Tungsten Oxynitrides: Synthesis, Characterization, and Catalytic Behavior in Propene Hydrogenation and *n*-Heptane Isomerization

P. Pérez-Romo, C. Potvin, J.-M. Manoli,[1] and G. Djéga-Mariadassou

Laboratoire Réactivité de Surface, Université Pierre et Marie Curie, CNRS UMR 7609, Case 178, 4 place Jussieu, 75252 Paris Cedex 05, France

Received July 5, 2001; revised September 20, 2001; accepted September 28, 2001

The effect of phosphorus on tungsten oxynitrides has been studied. Phosphorus was introduced via tungsten heteropolyanions. Propene hydrogenation and *n*-heptane isomerization were used to probe the activity and selectivity of the doped materials. Catalysts were characterized using elemental analysis, X-ray diffraction, N_2 BET surface area, CO chemisorption, and X-ray photoelectron spectroscopy (XPS). Reactivity experiments over P-containing oxynitrides show enhanced hydrogenating properties and decreased *n*-heptane isomerization. As indicated by XPS measurements, tungsten oxynitrides show higher concentrations of lower W oxidation states on P addition. © 2002 Elsevier Science

Key Words: **synthesis; characterization; tungsten oxynitride; heteropolyanion precursor; phosphorus.**

1. INTRODUCTION

Unsupported molybdenum nitrides with high specific area (1) have attracted a great deal of interest because of their excellent catalytic properties (2) and owing to their ability to replace noble metals catalysts (3) in several reactions. Many studies have demonstrated that molybdenum nitrides are effective and attractive hydrotreating (hydrodenitrogenation) catalysts (4–9). However, relatively few investigations have been devoted to the catalytic properties of bulk tungsten nitrides (10–12).

Phosphorus is frequently added to supported catalysts in order to improve the dispersion of the metal salts or the active-phase thermal stability or to modify the acid sites. Information on the catalytic effect of phosphorus on unsupported transition metal nitrides is limited (10, 13). Phosphorus can be added to the oxide form of the nitride precursors as a separate salt or as polyanionic compounds together with transition metal atoms (10, 13, 14). This method has the advantage of associating all elements in the same chemical unit. These doped materials have enhanced hydrogenation properties (14, 15).

[1] To whom correspondence should be addressed. Fax: +33 (0)1 44 27 60 33. E-mail: jmm@ccr.jussieu.fr.

The present study is based on an extension of our previous investigation (10). Several catalysts were prepared, using as starting materials ammonium polyanionic compounds with different P/W ratios (from 0 to 0.28). Catalysts were synthesized by a temperature-programmed reaction (TPR), then characterized and tested using two probe reactions: propene hydrogenation and *n*-heptane isomerization at atmospheric pressure. Elemental analysis, CO chemisorption, X-ray diffraction (XRD), BET surface area, and X-ray photoelectron spectroscopic (XPS) measurements were used to characterize the materials.

2. EXPERIMENTAL

Materials

Heteropolyanions with P/W atomic ratios ranging from 0 to 0.28 were purchased ($(NH_4)_6H_2W_{12}O_{40} \cdot xH_2O$ with P/W = 0 and $H_3PW_{12}O_{40} \cdot xH_2O$ with P/W = 0.08, Acros) or synthesized ($(NH_4)_6P_2W_{18}O_{62} \cdot xH_2O$ with P/W = 0.11, $(NH_4)_{12}P_2W_{12}O_{48} \cdot xH_2O$ with P/W = 0.17, and $(NH_4)_{12}P_4W_{14}O_{58} \cdot xH_2O$ with P/W = 0.28) according to the literature (16, 17) and used as precursors.

The gases employed were ammonia, propene, oxygen, and helium (all supplied by Air Liquide, 99.5%), hydrogen purified by passing through an oxygen trap (Oxysorb, Air Gaz), and argon (supplied by Air Liquide, 99.995%).

Catalyst Preparation

Tungsten oxynitrides were prepared using TPR of the precursors and ammonia, with a modification of the procedure described elsewhere (1). First the materials were heated quickly (heating rate 120 K h^{-1}) from room temperature to 673 K in flowing NH_3 (volume hourly space velocity from 15,000 h^{-1} to 23,000 h^{-1}). The materials were then nitrided using a lower linear heating rate (30 K h^{-1}), from 673 to 973 K. The samples were held at 973 K for 4 h. After rapid cooling to room temperature, the ammonia flow was

0021-9517/02 $35.00

switched to an O_2/Ar mixture (1% v/v) for a passivation step (10 L h^{-1} for 1 h).

Characterization

A gas chromatograph (GC) using a thermal conductivity detector (TCD) and an automatic injection valve were used to analyze the composition of the gas at the outlet of the preparation reactor. Nitrogen, hydrogen, and ammonia were separated on a 1 m × 1/8 in. Porapak Q column at 350 K with helium as carrier gas. A two-pen recorder was used to follow the progress of nitridation as a function of temperature.

All samples were first pretreated with flowing hydrogen in a quartz reactor at 773 K for 4 h before elemental analysis, BET, and XPS characterizations. They were then treated at 673 K under vacuum for 1 h and finally sealed in glass tubes. Elemental analyses were performed by the Service Central d'Analyse du Centre National de la Recherche Scientifique (Vernaison, France).

Specific surface areas (S_g) were determined using the N_2 BET method on a Micromeritics ASAP 2010 adsorption analyzer. The samples treated as described above were degassed under vacuum for 4 h on the Micromeritics unit prior to measurement. Pore-size distributions were determined from the N_2 desorption isotherms using the Barrett *et al.* cylindrical pore model (18).

A Siemens D500 automatic diffractometer with a CuK_α monochromated radiation source was used to determine the XRD patterns of the solid phases. The analysis included crystallite-size estimation from line broadening. The average crystallite size was calculated using the Scherrer formula (19): $D_{hkl} = 0.9\lambda/B\cos\theta$, where λ is the wavelength of the radiation, B the corrected peak width, and θ the Bragg angle of the peak. The crystallite size was taken as the average of D_{111} and D_{200}.

The selective chemisorption of CO was used to titrate active metallic sites before runs and was performed using a pulse technique at 293 K. A known volume of CO controlled by an automatic valve was passed through a quartz reactor containing the material (0.2–0.5 g), with He as carrier gas. A thermal conductivity detector detected the remaining nonadsorbed CO at the outlet of the reactor. Hence, the consumption of CO was determined and the amount of CO chemisorbed by the sample deduced. Samples of tungsten oxynitrides were first treated with flowing hydrogen in a quartz reactor at 773 K for 4 h, purged in flowing helium for 0.5 h, and then quenched at 293 K.

X-Ray Photoelectron Spectroscopy

X-ray photoelectron spectra were measured using a Surface Science Instrument SSX 100 spectrometer with a monochromated AlK_α X-ray source ($h\nu = 1486.6$ eV), a hemispherical electron analyzer, and a multichannel detector. Sealed glass tubes were opened in a glove box (dry argon) connected to the XPS spectrometer. Materials were transferred to the sample holder and introduced into the spectrometer chamber without exposure to air. Samples were then outgassed in the pretreatment chamber at 10^{-5} Torr prior to transfer to the analysis chamber. The vacuum applied during the measurements was typically less than 5×10^{-9} Torr and data were accumulated in separate regions. The C 1s peak of the contamination carbon (binding energy (BE) = 284.6 eV) was taken as reference in calculating BEs and accounting for charging effects. Experimental peaks were decomposed into components (90% Gaussian, 10% Lorentzian) using a nonlinear, least-squares fitting algorithm and a Shirley baseline. The W 4f spectra typically consisted on an envelope of peaks which were decomposed to estimate the W oxidation-state distribution. To reconstruct the levels of tungsten, some parameter constraints were imposed. A splitting energy of 2.1 eV and an intensity ratio $I(\mathrm{W\ 4f_{5/2}})/I(\mathrm{W\ 4f_{7/2}}) = 0.75$ (20) were used for the W $4f_{5/2}$–W $4f_{7/2}$ doublet. Both peaks of the doublet were constrained to have the same full width at half the maximum peak height. For all elements, atomic concentrations were estimated based on comparisons of integrated peak intensities normalized by the atomic sensivity factors (20). BEs were reproducible to within ±0.2 eV.

Propene Hydrogenation

Propene hydrogenation was chosen as a model reaction to determine the hydrogenation properties of materials at atmospheric pressure. The reaction was carried out at 353 or 423 K, depending on the activity of the catalyst. Prior to each run, passivated catalysts were pretreated *in situ* at 773 K in flowing H_2 (0.72 L h^{-1}) for 5 h. The catalyst weight was chosen in order to obtain a conversion lower than 10%, allowing the assumption of a pseudo-zeroth order for propene. The gas mixture (the H_2/C_3H_6 molar ratio was fixed at 6.7 and the total flow rate at 6.9 L h^{-1}) was fed into a Pyrex reactor loaded with 0.02–0.15 g of catalyst on a sintered glass disk (1 cm in diameter). The effluent composition was analyzed with a HP 5890 series II gas chromatograph equipped with a KCl-modified Al_2O_3 capillary column and a flame ionization detector. The only product observed was propane. As the catalysts suffered deactivation during reactions, the initial conversion was determined according to a second-order deactivation law: the reciprocal value of the conversion, τ, versus time of run, t, was used to determine the initial conversion, τ_0, by extrapolation to zero time: $1/\tau = 1/\tau_0 + \kappa t$, where κ is an empirical deactivation constant (21).

Selective Isomerization of n-Heptane

The *n*-heptane reaction was carried out at 623 K (atmospheric pressure) and its partial pressure (42.3 Torr) was provided by a saturator kept at a suitable temperature. The

H_2/n-C_7H_{16} molar ratio was fixed at 17 (catalyst weight 0.07 g) and the total flow rate at 0.75 L h^{-1}.

The composition of the effluent was analyzed using an online gas chromatograph system consisting of a 50-m HP-PONA capillary column coated with methylsiloxane. The total conversion reached steady state activity after 5 h on stream; the catalytic conversion and selectivity were measured at the steady state, the selectivity for the isomer products being defined as the percentage of *n*-heptane converted to isoheptanes. Passivated samples were treated in the same way as for propene hydrogenation.

3. RESULTS AND DISCUSSION

Ammonia Decomposition during Preparation: TPR Experiments

During temperature-programmed nitridation the gas-phase concentrations of NH_3, N_2, and H_2 were monitored by GC. The plot for N_2 formation followed that for NH_3 disappearance and therefore is not shown in Fig. 1. Ammonia was decomposed on the precursor samples using the nitriding parameters given above (see Experimental). Plots show the TCD signal for NH_3 and the temperature versus time of run (Fig. 1). Decomposition of ammonia began at about 750 K for all precursors and it was evident that all the materials with different P/W ratios followed the same reduction route. The nitrogen (N species) of the decomposed NH_3 began to replace the oxygen of the oxide lattice, oxynitride being therefore produced at this point. The NH_3 decomposition was similar to that on ammonium metatungstate for all precursors with a P/W ratio lower than or equal to 0.11 (curve a). However the entire process for the compounds mentioned was shifted to a lower temperature by about 80 K compared to the precursor with P/W = 0.28 (curve c). Ammonia decomposition was complete at 973 K for tungsten oxynitride and oxynitrides with a P/W ratio lower than or equal to 0.11 (curve a). The other oxynitrides with a higher phosphorus content (curves b and c) were less active, suggesting a surface area influence. At 973 K the maximum of active surface sites was reached for each material synthesized and stable catalytic decomposition of ammonia occurs. The heating rates and final temperature were chosen according to these observations.

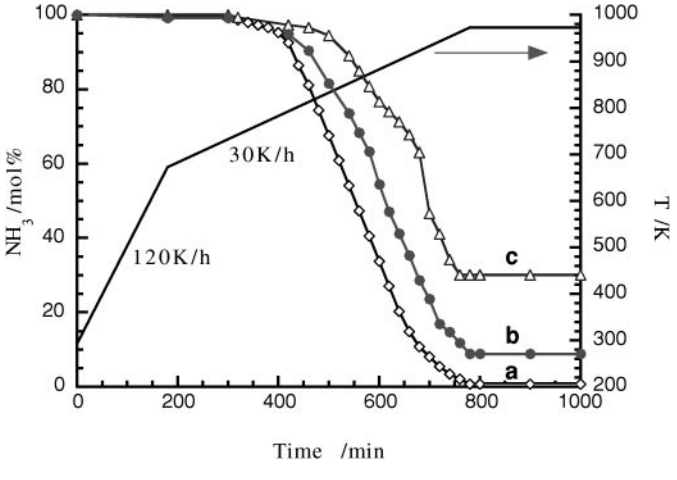

FIG. 1. Changes in NH_3 chromatographic peaks as a function of time and temperature during ammonia treatment (6 L h^{-1}) of the following precursors: P/W ≤ 0.11 (a), P/W = 0.17 (b) , P/W = 0.28 (c). Temperature gradient 120 K h^{-1} or 30 K h^{-1}.

TABLE 1

Physical Properties of Tungsten Oxynitrides

Precursor	P/W ratio	Chemical analysis formula	Surface area S_g (m^2 g^{-1})	Surface area Pore size (nm)	Crystallite size [D_c (nm)]
$H_2W_{12}O_{40}$ $(NH_4)_6$	0	$WN_{1.08}O_{0.48}$	74	4.0–8.0	4.2
$H_3PW_{12}O_{40}$	0.08	$WN_{1.28}O_{1.67}P_{0.09}$	87	3.5	3.8
$P_2W_{18}O_{62}$ $(NH_4)_6$	0.11	$WN_{1.10}O_{0.48}P_{0.11}$	64	2.0	2.3
$P_2W_{12}O_{48}$ $(NH_4)_{12}$	0.17	$WN_{1.00}O_{0.44}P_{0.16}$	33	2.7	2.2
$P_4W_{14}O_{58}$ $(NH_4)_{12}$	0.28	$WN_{1.09}O_{0.8}P_{0.28}$	44	2.7	2.1

Influence of Phosphorus on XRD of Materials

The elemental analysis results (Table 1) show a higher amount of oxygen in all cases, with a metal/(N + O) ratio lower than the theoretical formula required for tungsten nitride (W_2N). We present the chemical formulae of these materials as WN_xO_y or $WN_xO_yP_z$ and refer to them as oxynitrides. The P/W ratios are the same before and after the nitridation process (Table 1).

The XRD results for the various materials synthesized are presented in Fig. 2. Two of the oxynitrides reported here have a similar five-peak XRD patterns (only four are visible for the others). Comparison with a standard pattern from a powder diffraction file indicates that these compounds can be identified as β-W_2N (JCPDS 25-1257). Calculation yields a value of 0.4161 (4) nm for the lattice parameter a_0, slightly greater than for β-W_2N ($a_0 = 0.4126$ nm). Tungsten nitride presents a NaCl-like cubic structure with the metal atoms in a face-centred cubic (fcc) arrangement and N filling only half the available octahedral sites. Kiessling and Peterson (22) and more recently Lucy *et al*. (11) reported the formation of a tungsten oxynitride with a defective NaCl-like structure (space group Fm3m) by the reaction of WO_3 with NH_3 at 973 K. According to the chemical formulae, these compounds clearly lack tungsten atoms but preserve the XRD pattern of the fcc β-W_2N. As proposed by Kiessling and Peterson (22), the most probable explanation is that the nonmetal atoms O and N together occupy all the octahedral positions of the cubic unit lattice, whereas there are vacancies in the metal sublattice of the NaCl-like structure. Vacancies exist also in the sublattice of molybdenum in the molybdenum oxynitrides, as shown by

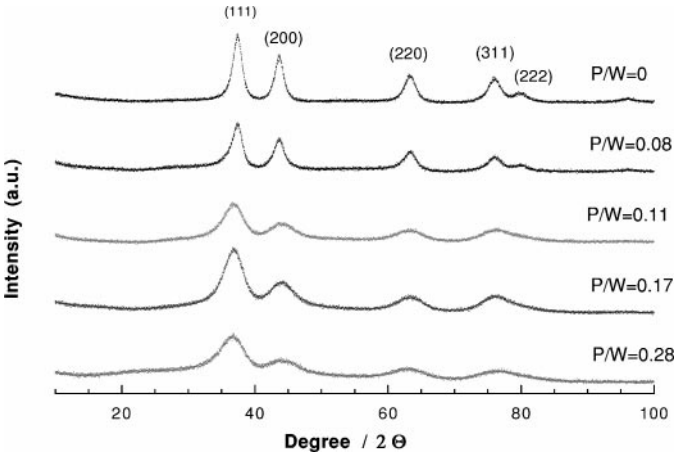

FIG. 2. X-ray diffraction patterns of tungsten oxynitrides prepared using different heteropolyanions.

Gouin *et al*. (23) from density measurements. The chemical formulae of our materials are consistent with those proposed in the literature for $WN_{1.0}O_{0.6}$ (22) and $WN_{0.8}O_{0.6}$ (11). The slight increase in the lattice parameter can be explained by the presence of oxygen or is due to the fact that the nitrogen content of the oxynitrides prepared here is higher than that of β-W_2N. Addition of phosphorus still maintains the fcc crystal structure of β-W_2N but a consequent peak broadening is observed with increasing P/W content. Moreover, the crystallite size (D_c) calculated by the Scherrer formula based on XRD peak broadening indicates a particle size of about 4.2 to 2.1 nm, decreasing as the amount of phosphorus increases and suggesting finely divided powders.

Evolution of the Specific Surface Area: Influence of the P/W Ratio

The specific surface areas and average pore sizes for tungsten oxynitrides prepared from different precursors are summarized in Table 1. Tungsten oxynitride produced from the P-free precursor gave a specific surface area in agreement with those reported in previous publications (1, 11, 12, 24, 25). Compounds can be divided into two groups, the first containing materials with a P/W ratio up to and including 0.11, and the other with higher P contents. No noticeable difference was observed in the specific surface areas for the first group, whereas the second group showed about a 50% decrease. Pore-size distribution for $WN_{1.08}O_{0.48}$ was bimodal, pore sizes for the other materials being between 2 and 4 nm, in the mesopore range. It is reasonable to assume that the small tungsten oxynitride particles were agglomerated, leading to a mesoporouslike, interparticular system. It is interesting to note that in the case of molybdenum nitrides a higher decrease in the specific surface area was observed by Li and Lee (13) (from 175 $m^2\ g^{-1}$ for Mo_2N down to 48 $m^2\ g^{-1}$ for P-containing material with a P/Mo ratio of only 0.08).

CO Chemisorption for Titration of Noble Metal-like Surface W Atoms

Carbon monoxide is commonly used as a molecular probe to titrate the number of accessible surface metal atoms. As shown in Table 2, the CO uptakes of the current samples range from low (40.6 μmol g^{-1}) to medium (149 μmol g^{-1}) values, assuming molecular adsorption and hence 1 : 1 stoichiometry between CO and the exposed adsorbing tungsten atoms for tungsten oxynitride. If a stoichiometric fcc lattice structure is assumed, a density of about 1×10^{15} W atoms per square centimeter can be calculated. The values obtained (Table 2) in this study are in the range 0.07–0.11 $\times 10^{15}$ cm^{-2}, indicating that 7–11% of the surface tungsten atoms are chemisorbing CO. These values are slightly smaller than those reported for molybdenum oxynitrides and are consistent with the values calculated for tungsten oxynitrides (11). It appears that the presence of P in tungsten oxynitride lowers the surface area moderately and concomitantly reduces CO chemisorption. Furthermore, the results indicate a linear relation between surface area and CO uptake; consequently, almost the same number of accessible surface atoms per square meter is observed whatever the P-content. The nonstoichiometry in the metal lattice (lack of tungsten) can explain the low uptake observed in this and previous work (13).

XPS Analysis

The XPS technique was used in order to obtain information regarding the oxidation states of the surface tungsten atoms. To our knowledge, XPS results concerning tungsten oxynitrides are rare, whereas XPS results for tungsten carbides have been widely reported (26, 27). The W 4f spectra typically consist of an envelope of peaks which was decomposed in order to estimate the W oxidation-state distribution. The XPS spectra in the W 4f region for all the catalysts are presented in Fig. 3. The BEs

TABLE 2

CO Chemisorption and Comparison of Turnover Rates (TOR) for Propene Hydrogenation over Tungsten Oxynitrides

Tungsten oxynitrides	P/W ratio	CO chemisorption		TOR (s^{-1})	
		Uptake (μmol g^{-1})	Site density ($\times 10^{15}$ cm^{-2})	353 K	423 K
$WN_{1.08}O_{0.48}$	0	136	0.11	—	0.018
$WN_{1.28}O_{1.67}P_{0.09}$	0.09	149	0.10	0.012	—
$WN_{1.10}O_{0.48}P_{0.11}$	0.11	116	0.11	0.25	—
$WN_{1.00}O_{0.44}P_{0.16}$	0.16	41	0.07	0.15	—
$WN_{1.09}O_{0.8}P_{0.28}$	0.28	81	0.11	0.13	—

of the various elements and the percentages of the different oxidation states of tungsten are summarized in Table 3. Three W species were detected after nitridation. No contribution at the lowest binding energy corresponding to W metal (30.6 eV) was detected (28) in any compound. The various materials used fell into two classes with respect to their P/W ratios: the first consisted of the P-free and the P/W = 0.08 heteropolyacid precursors, leading to similar binding energies for the W species, and the second corresponded to high P/W ratio materials (from 0.11 to 0.28). A typical decomposed XPS spectrum for the first class of materials is shown in Fig. 4: three W species are identified, the highest BE being the fingerprint of W^{6+}, as in WO_3. Following previous studies (29, 30) we assigned the BE at 33.9–33.8 eV to W^{5+}, whereas the lowest contribution detected at 32.8–32.9 eV could be identified as W^{4+} (30). Consequently, the results suggest that these two oxynitrides contain mainly amorphous oxide domains at the surface. For the second class of materials (high P/W ratios, above 0.11), three W species were also observed; with the exception of the highest BE peak, the two others were shifted toward lower BEs. The peak at high energy was attributed to W^{6+}, as previously suggested, while the values at 32.9–33.5 eV were assigned to W^{4+} (30). The BE of the species at lower energy was midway between those for W^0 and W^{4+}: this species was denoted $W^{\delta+}$, where $0 < \delta < 4$.

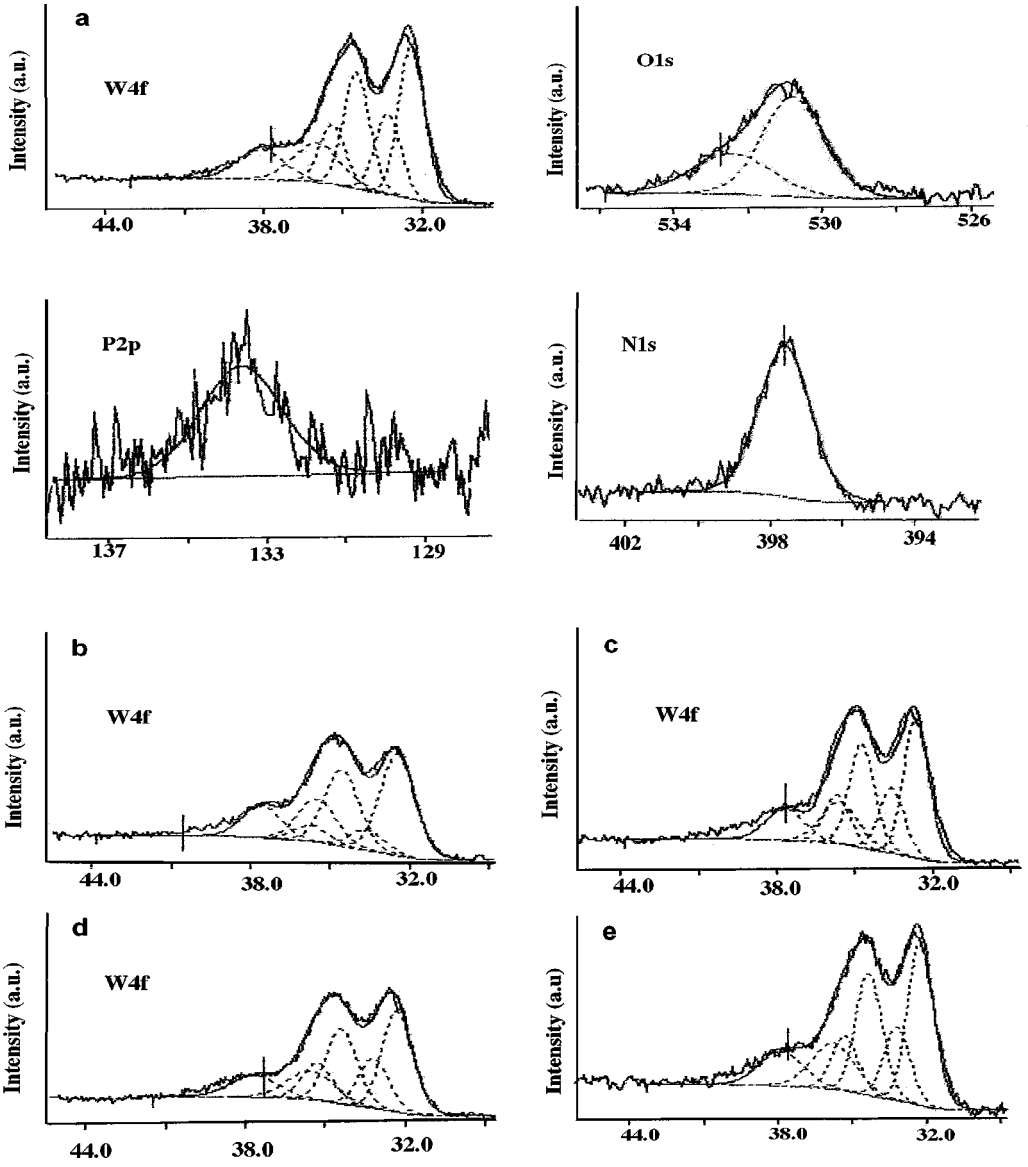

FIG. 3. Superposition of the experimental XPS spectra and spectra after decomposition for tungsten oxynitride samples: $WN_{1.10}O_{0.48}P_{0.11}$ (P/W = 0.11) (a) at the W 4f, O 1s, N 1s, and P 2p levels and at the W 4f level for $WN_{1.08}O_{0.48}$ (P/W = 0) (b); $WN_{1.28}O_{1.67}P_{0.09}$ (P/W = 0.09) (c); $WN_{1.00}O_{0.44}P_{0.16}$ (P/W = 0.16) (d); and $WN_{1.09}O_{0.8}\ P_{0.28}$ (P/W = 0.28) (e).

TABLE 3

X-Ray Photoelectron Spectroscopy Analysis of Tungsten Oxynitrides with Different P/W Ratios

P/W	O 1s Oxide		N 1s Nitride		P 2p		W $4f_{7/2}$ $W^{\delta+}$	W^{4+}	W^{5+}	W^{6+}
0	530.7	532.3	397.7	399.8				32.8 (59%)	33.9 (13%)	35.8 (28%)
0.08	531.0	532.8	397.6	398.6	133.0	134.5		32.9 (49%)	33.8 (25%)	36.0 (26%)
0.11	531.0	532.6	397.8		133.8		32.6 (51%)	33.5 (26%)		36.2 (23%)
0.17	530.7	532.3	397.3	398.6	133.3		32.3 (52%)	33.2 (26%)		35.5 (22%)
0.28	530.4	532.1	396.9	398.1	133.0		31.9 (51%)	32.9 (24%)		35.5 (24%)

Note. Binding energies (eV) and concentration (%) of $W4f_{7/2}$ species. The number in brackets represents the percentage area of the W species.

$W^{\delta+}$ has been observed in tungsten carbide, and in our materials was involved in a W–N bond. In conclusion, it can be seen that phosphorus added via heteropolyanion precursors in our materials reduced (with the exception of W^{6+}) the BE of the W species. A linear relationship (Fig. 4) can be drawn between the lowest BE and the P/W ratio; these results clearly indicate that tungsten atoms in tungsten oxynitrides became more and more metallic as the P/W ratio was increased. The two peaks in the deconvoluted N 1s spectra for high P/W ratios were due to two types of structural nitrogen species. The less energetic one corresponding to BEs ranging from 397.8 to 396.9 eV was ascribed to nitride species linked to tungsten atoms (31, 32). The peaks at higher energy (398.1–398.6 eV) were assigned to P–N bonds, as reported in the comparison with data given in the literature by Fripiat *et al*. (31). The 399.8-eV component observed in the P-free material can be attributed to NH_x species adsorbed on Lewis sites (33) and in particular to $–NH_2$ species (34). From all these data, the presence of less-energetic peaks for the high P-containing tungsten oxynitrides excluded the presence of significant acidic adsorption sites.

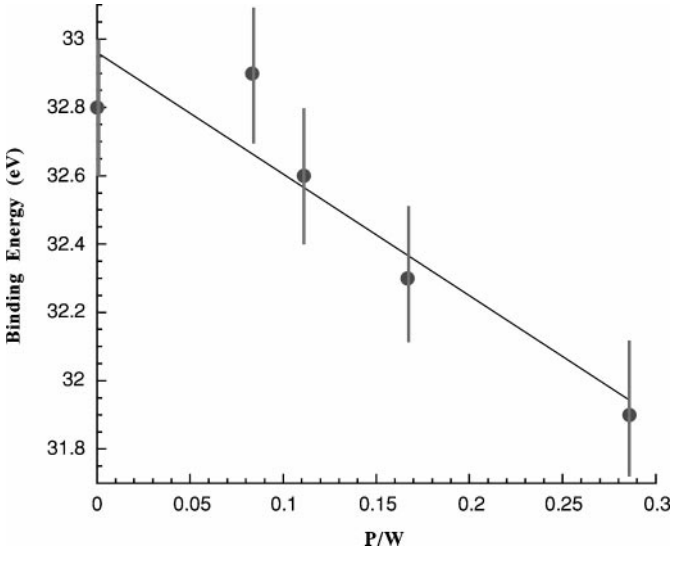

FIG. 4. Lowest binding energy of tungsten species (W $4f_{5/2}$) as a function of P/W ratio for tungsten oxynitrides.

The region of the O 1s spectra included two peaks. It is generally accepted that peaks at about 530 eV are due to oxides and that at about 532 eV to adsorbed oxygen species such as O^-, OH^-, or H_2O (35).

The P 2p profiles of P-containing materials were similar, with the exception of the large P 2p peak for the 0.08 P/W ratio, which can be decomposed into two peaks, indicating that there are two kinds of P species, with binding energies of 133 and 134.5 eV. These components with high binding energies of about 133–134 eV were assigned to P–O (36, 37) or P–N bonds, as also reported by Li and Lee (7, 38). As seen in Table 3, P 2p peaks were displaced to lower values as the P/W ratio was raised. Such behavior was reported by Brow *et al.* (39) in PON solids. This shift is believed to be due to replacement of P–O bonds by P–N bonds, the average ionic charge on the phosphorus ion being reduced when nitrogen replaces oxygen. No reduced phosphorus species such as phosphides (130 eV for the P 2p region) were observed.

Hydrogenation Properties

Propene hydrogenation (a structure-insensitive reaction) was selected as a molecular probe reaction to evaluate the role of phosphorus on the hydrogenation activity of tungsten oxynitrides. Activity measurements were conducted at 353 K. For the sake of comparison, an experiment was performed at 423 K over tungsten oxynitride containing no phosphorus and showing very poor hydrogenating activity. The specific rate (micromoles per second per gram of catalyst) could be deduced from the initial conversion; assuming that active sites are titrated by CO, a propene hydrogenation turnover rate (TOR) could therefore be easily obtained.

As observed (Table 2), the P-containing catalysts had higher propene hydrogenation TOR than those without. Furthermore, as for the XPS experiments, two groups of materials were distinguished. The group with P/W ratios

going from 0.11 to 0.28 displayed turnover rates at least 10 times higher than those of the other compounds, with P/W = 0 or 0.08. Consequently, from the XPS (reduction of the BE of $W^{\delta+}$) and TOR results, it can be deduced that the hydrogenation character of tungsten oxynitrides is strongly linked to the presence of phosphorus.

Isomerization Properties

The isomerization of *n*-heptane was carried out to test the capacity of these new materials in isomerization processes. As shown in Table 4, the selectivity to isomer products was around 90% for the P-free tungsten oxynitrides, the major isomers being monomethylhexanes. When phosphorus was added to tungsten oxynitrides, conversion and heptane isomerization were lowered, and the amount of $C_3 + C_4$ products decreased while the $C_1 + C_6$ products increased, suggesting a shift from cracking to hydrogenolysis. Tungsten oxynitride was obviously bifunctional and capable of isomerizing *n*-heptane, giving a substantial amount of monobranched and dibranched C_7 isomers. We propose that oxygen present on the surface (oxynitride-synthesized materials or passivation treatment) induced Brønsted acid sites required in isomerization reactions, as previously reported for oxygen-exposed tungsten carbides (40) and suggested by the XPS experiments (presence of W^{6+}, W^{5+}, and W^{4+}). The tungsten oxynitride with the highest P/W ratio exhibited significantly lower isomerization selectivity and an increase in cyclic C_7 isomers, ethylpentane, and $C_1 + C_6$ products, indicating enhanced metallic activity.

These observations are in agreement with the propene hydrogenation results: the incorporation of an increasing amount of phosphorus in tungsten oxynitrides shifts the catalytic behavior toward that of a more metallic material, improving the hydrogenating properties (metallic function) relative to acidic properties.

TABLE 4

Product Distribution for the Conversion of *n*-Heptane on Phosphorus-Modified Tungsten Oxynitrides after 5 h on Stream at 623 K

P/W	0	0.08	0.11	0.17	0.28
Conv. (%)	11.1	6.3	4.4	3.9	4.4
Isomer select (%)	89.1	86.1	48.9	29.7	21.2
Isomer. products (%)					
MHex	82.1	78.2	84.2	73.8	57.0
DMP	11.3	13.8	1.3	1.0	0.0
EtP	0.7	1.0	3.8	11.6	11.2
$\sum$cyclic	5.9	6.9	10.7	13.6	32.8
2MHex/3MHex	0.82	0.75	0.73	0.82	0.93
$C_1 + C_6$	19.5	20.4	23.7	27.2	31.4
$C_2 + C_5$	32.8	39.1	38.4	40.3	36.2
$C_3 + C_4$	47.6	40.3	37.9	32.5	32.4

Note. DMP, sum of dimethylpentanes; 2MHex or 3MHex, 2- or 3-methylhexane; EtP, ethylpentane.

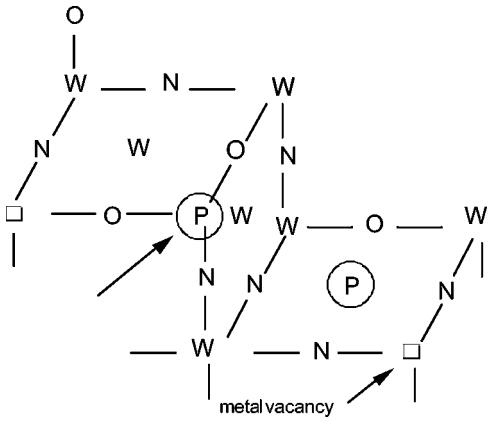

FIG. 5. Oversimplified model for $WO_xN_yP_z$: metallic site (W, P, vacancy) and octahedral site (N, O).

Model for Tungsten Oxynitride Doped with Phosphorus

A tungsten phosphide WP was prepared using TPR of an X-ray-amorphous tungsten phosphate by Clark *et al.* (41). Comparison of our XRD patterns with that of WP establishes that tungsten phosphide was not present in our materials. The observation of P 2p binding energies at about 133–134 eV attributed to phosphate and the absence of any peak at 129–130 eV associated with P bonded to metal also argues against phosphide. Nuclear magnetic resonance measurements on tungsten oxynitrides doped with phosphorus and mixed with KBr (the metallic character of these materials prevents any measurements with bulk compounds) showed a ^{31}P resonance at −13.3 ppm; no chemical shift (from +200 to +300 ppm) corresponding to phosphide (42) was observed.

These studies by various physicochemical techniques show without doubt the presence of phosphate in our materials, but no conclusion about the inhomogeneous (biphasic) or homogeneous character of these compounds can be given at this stage. However, the catalytic properties (hydrogenation and isomerization) of these oxynitrides are strongly dependent on the P/W ratio.

Taking into account these data, we suggest an oversimplified model valid for the core of the phosphorus-containing oxynitrides derived from that proposed to illustrate the concept of dual sites in MoN_xO_y (8, 9). As shown in Fig. 5, phosphorus atoms filled some of the metal vacancies, leaving the O and N atoms occupying all the octahedral sites. The higher metallic nature of the tungsten following the increasing P/W ratio can be explained by the existence of phosphorus oxynitride layers reducing the positive charge around the tungsten atoms.

4. CONCLUSION

For the first time new P-containing tungsten oxynitrides have been synthesized from various heteropolyanion

precursors and characterized by chemical analysis, XRD, and CO chemisorption.

The XPS data show that the reducibility of the tungsten species increases when phosphorus is present. The catalytic properties are greatly modified by the presence of phosphorus; it enhances the turnover rates in propene hydrogenation and decreases the selectivity for *n*-heptane isomerization (mono- and dimethyl isomers).

ACKNOWLEDGMENTS

P. Pérez-Romo is grateful to the Consejo Nacional de Ciencia y Tecnologia (CONACyT) for financial support. The help of M. Leclerc and P. Bargiela with the XPS measurements is greatly appreciated. We thank Dr. J. S. Lomas for constructive discussions and for correcting the manuscript.

REFERENCES

1. Volpe, L., and Boudart, M., *J. Solid State Chem*. **59**, 332 (1985).
2. Oyama, S. T., Schlatter, J. C., Metcalfe, J. E., and Lambert, J. M., *Ind. Eng. Chem. Res*. **27**, 1639 (1988).
3. Levy, R. B., and Boudart, M., *Science* **181**, 457 (1973).
4. Schlatter, J. C., Oyama, S. T., Metcalfe, J. E., and Lambert, J. M., *Ind. Eng. Chem. Res*. **27**, 1648 (1988).
5. Thompson, L. T., Colling, C. W., Choi, D., Demczyk, B. G., and Choi, J.-G., *in* "New Frontiers in Catalysis" (L. Guczi, F. Solymosi, and P. Tétényi, Eds.), p. 941. Elsevier, Amsterdam, 1993.
6. Nagai, M., Goto, Y., Uchino, O., and Omi, S., *Catal. Today* **43**, 249 (1998).
7. Li, S., and Lee, J. S., *J. Catal*. **173**, 134 (1998).
8. Stanczyk, K., Kim, H. S., Sayag, C., Brodzki, D., and Djéga-Mariadassou, G., *Catal. Lett*. **53**, 59 (1998).
9. Miga, K., Stanczyk, K., Sayag, C., Brodzki, D., and Djéga-Mariadassou, G., *J. Catal*. **183**, 63 (1999).
10. Sellem, S., Potvin, C., Manoli, J.-M., Contant, R., and Djéga-Mariadassou, G., *J. Chem. Soc., Chem. Commun*. 359 (1995).
11. Lucy, T. E., St. Clair, T. P., and Oyama, S. T., *J. Mater. Res*. **13**, 2321 (1998).
12. Neylon, M. K., Choi, S., Kwon, H., Curry, K. E., and Thompson, L. T., *Appl. Catal. A* **183**, 253 (1999).
13. Li, S., and Lee, J. S., *J. Catal*. **162**, 76 (1996).
14. Pérez-Romo, P., Potvin, C., Manoli, J.-M., and Djéga-Mariadassou, G., *Stud. Surf. Sci. Catal*. **130**, 2855 (2000).
15. Da Costa, P., Potvin, C., Manoli, J.-M., Breysse, M., and Djéga-Mariadassou, G., *Catal. Lett*. **72**, 91 (2001).
16. Contant, R., *in* "Inorganic Syntheses" (P. Ginsberg, Ed.), p. 104. Wiley, New York, 1990.
17. Thouvenot, R., Tézé, A., Contant, R., and Hervé, G., *Inorg. Chem*. **27**, 524 (1988).
18. Barret, E. P., Joyner, L. G., and Halenda, P. P., *J. Am. Chem. Soc*. **73**, 376 (1951).
19. Scherrer, P., *Nachr. Ges. Wiss. Göttingen* **26**, 198 (1918).
20. Seah, M. P., *in* "Practical Surface Analysis by Auger and X-ray Photoelectron Spectroscopy" (D. Briggs and M. P. Seah, Eds.), Vol. 1, Chap. 5, pp. 225–226. Wiley, New York, 1990.
21. Germain, J. E., and Maurel, R., *C. R. Acad. Sci*. **247**, 1854 (1958).
22. Kiessling, R., and Peterson, L., *Acta Metall*. **2**, 675 (1954).
23. Gouin, X., Marchand, R., L'Haridon, P., and Laurent, Y., *J. Solid State Chem*. **109**, 175 (1994).
24. Kim, J. H., and Kim, K. L., *Appl. Catal. A* **181**, 103 (1999).
25. Cho, D.-H., Chang, T.-S., and Shin, C.-H., *Catal. Lett*. **67**, 163 (2000).
26. Nakasawa, M., and Okamoto, H., *Appl. Surf. Sci*. **24**, 75 (1985).
27. Ledoux, M. J., Pham Huu, C., Guille, J., and Dunlop, H., *J. Catal*. **134**, 383 (1992).
28. Ramqvist, L., Hamrin, K., Johansson, G., Fahlman, A., and Nordling, C., *J. Phys. Chem. Solid* **30**, 1835 (1969).
29. Katrib, A., Hemming, F., Wehrer, P., Hilaire, L., and Maire, G., *J. Electron. Spectrosc. Relat. Phenom*. **76**, 195 (1995).
30. Katrib, A., Logie, V., Saurel, N., Wehrer, P., Hilaire, L., and Maire, G., *Surf. Sci*. **377–379**, 754 (1997).
31. Fripiat, N., Centeno, M.-A., and Grange, P., *Chem. Mater*. **11**, 1434 (1999).
32. Fix, R., Gordon, R. G., and Hoffman, D. M., *Chem. Mater*. **5**, 614 (1993).
33. Leung, Y. L., Wong, P. C., Zhou, M. Y., Mitchell, K. A. R., and Smith, K. J., *Appl. Surf. Sci*. **136**, 178 (1998).
34. Liu, H., Bertolet, D. C., and Rogers, J. W., *Surf. Sci*. **340**, 88 (1995).
35. Choi, J.-G., and Thompson, L. T., *Appl. Surf. Sci*. **93**, 143 (1996).
36. Massinon, A., Guéguen, E., Conanec, R., Marchand, R., Laurent, Y., and Grange, P., *Stud. Surf. Sci. Catal*. **101**, 77 (1996).
37. Benitez, J. J., Centeno, M.-A., Odriozola, J. A., Conanec, R., Marchand, R., and Laurent, Y., *Catal. Lett*. **34**, 379 (1995).
38. Li, L., and Lee, J. S., *J. Catal*. **178**, 119 (1998).
39. Brow, R. K., Reidmeyer, M. R., and Day, D. E., *J. Non-Cryst. Solids* **99**, 178 (1988).
40. Iglesia, E., Baumgartner, J. E., Ribeiro, F. H., and Boudart, M., *J. Catal*. **131**, 523 (1991).
41. Clark, P., Li, W., and Oyama, S. T., *J. Catal*. **200**, 140 (2000).
42. Prins, R., private communication.